Clays Clay Miner., Vol. 70, No. 5:695–711, 2022
https://doi.org/10.1007/s42860-022-00211-7

ORIGINAL PAPER

Occurrence of Iron in the Minerals of Carboniferous Coal Gangue of the Pingshuo Open-pit Mine, North China

Lihui Liu · Qinfu Liu · Yakui Li · Haiyue Cao · Xingjian Kang

Accepted: 26 October 2022 / Published online: 7 December 2022

Abstract The state of iron in coal gangue minerals is an important factor in determining the potential for value-added utilization of this solid waste; this is especially true for the coal gangue coming from the Pingshuo open-pit mine in China. The objective of the present study was to characterize the petrological, mineralogical, and chemical states of Fe in the coal gangue from the Carboniferous Taiyuan Formation. Methods used included polarizing microscopy, X-ray diffraction (XRD), scanning electron microscopy–energy-dispersive spectroscopy (SEM–EDS), X-ray fluorescence, micro-Fourier-transform infrared (micro-FTIR) spectroscopy, and Mössbauer spectroscopy. The coal gangues are mudstones, silty mudstones, and pelitic siltstones, which are composed primarily of kaolinite, quartz, feldspar, pyrite, illite, and magnesite. In coal gangue, the Fe was found to occur in ferruginous minerals, in crystal-lattice substitutions, or in a colloidal state. The ferruginous minerals in the coal gangue are pyrite and marcasite, and the pyrite morphologies are framboidal, euhedral octahedral crystals, subhedral granular crystals, and irregular crystals. The results of SEM–EDS and micro-FTIR confirmed that the lattice substitution of Fe in the coal gangue minerals occurred mainly in kaolinite, resulting in two types of kaolinite: iron-containing and iron-free kaolinite. The former may be transformed from volcanic biotite and the latter from volcanic feldspar. The Mössbauer spectra of kaolinite showed intense doublets with isomer shift and quadrupole splitting values consistent with tetrahedrally coordinated Fe^{3+} and ocahedrally coordinated Fe^{2+}, suggesting the presence of two types of substitution sites: (1) Fe^{2+} replacing Al^{3+} in the octahedral sheet; and (2) Fe^{3+} replacing Si^{4+} in the tetrahedral sheet. This study has important theoretical significance for the high-value utilization of coal gangue.

Keywords Coal gangue · Colloidal state · Kaolinite · Lattice substitution · Pyrite

Introduction

Coal gangue is the mixture of rocks discharged during coal mining and processing, and is generally viewed as solid waste. According to data from the National Development and Reform Commission, coal output was 3.9 billion tons and coal gangue output was 795 million tons in China in 2021. The high-value comprehensive utilization rate of coal gangue in China is low. In terms of the current production rate and treatment mode, coal gangue is still one of the largest industrial solid wastes in China (Liu et al., 2013).

Associate editor: Yuji Arai

L. Liu · Q. Liu (✉) · Y. Li · H. Cao · X. Kang
School of Geosciences and Surveying Engineering,
China University of Mining &Technology (Beijing),
Beijing 100083, China
e-mail: lqf@cumtb.edu.cn

The characteristics of coal gangue depend mainly on their location and environment of formation of coal seams. Coal gangue contains harmful elements, such as Mn, Ag, Cd, Li, Ga, Hg, Ni, Pb, As, etc. (Dai et al., 2002; Ribeiro et al., 2010). Rainfall causes these pollutants to be leached into the surrounding soil or to enter bodies of water, resulting in environmental pollution (Shao, 2007; Stracher & Taylor, 2004). A coal gangue hill exposed to air will combust spontaneously and release a large amount of harmful gases, such as SO_2 and CO_2 (Cheng et al., 2013; Ozdeniz et al., 2010; Spears et al., 1994). Therefore, there is an urgent need to make better use of coal-gangue resources and eliminate their negative impacts on the environment (Pone et al., 2007; Querol et al., 2011).

The material composition of coal gangue determines how it can be used. For example, pyrite associated with coal gangue can be recovered by gravity or magnetic separation to achieve improved economic return. In recent years, most coal gangues have been used for power generation, brick making, cement, and so on (Cao et al., 2021a, 2021b; Li & Wang, 2019). However, these uses are not of very high value, so, over the past two decades, a large amount of coal gangue, which is kaolinite-rich claystone in coal measures, has been used in northern China as a raw material for the manufacture of calcined kaolin for fillers and coatings in paper making and in pigments. However, the occurrence and amount of iron in kaolinite-rich coal gangues restrict processing technologies in these industries and, in particular, diminish the whiteness of calcined kaolin and its deep-processing products (Bertolino et al., 2010; Gonzalez & Ruiz, 2006). Iron is common in kaolinite from coal measures, either as an isomorphically substituted ion in the kaolinite structure or as a stain from (oxyhydr)oxide coating. The form of iron available has a significant influence on the lattice defects and physicochemical properties of the minerals (Kramer et al., 2010; Lu et al., 2015).

Although many studies have characterized coal gangue and pyrite in coals (Meng et al., 2013; Soliman & Goresy, 2012; Yani & Zhang, 2010; Zhou et al., 2012), most of them are about the genesis of pyrite and the analysis of phase transformation during coal combustion. Studies of the detailed resource characteristics of iron in coal gangue are rare. Understanding the characteristics of the minerals is a prerequisite for high-value utilization. The purpose of the current study was to determine the state of Fe in the coal gangue from the Pingshuo open-pit mine in northern China to enable: (1) characterization of the various iron-bearing minerals in the coal gangue; (2) determination of the various forms of Fe in the constituent kaolinite; and (3) provision of a theoretical basis for the high-value utilization of iron-bearing minerals or kaolinite in coal gangue.

Geological Background

The study area of the Pingshuo open-pit mine is located in the north of the Ningwu Coalfield, Shanxi Province, China. The coalfield is long from north to south and narrow from east to west, exhibiting a northeast syncline. It is an inherited superimposed tectonic basin between the Lvliang, Wutai, and Inner Mongolian axes. The basement of the Ningwu coalfield is a set of ancient metamorphic rock series, with the sedimentary center located in the Ningwu-Jingle area in the south-central part of the coalfield. The total thickness of sedimentation is >3500 m. According to the stratigraphic sequence, the strata exposed and drilled in the mine field range in age from Cenozoic: Quaternary and Neogene; Mesozoic: Jurassic and Triassic; Paleozoic: Permian, Carboniferous; to Ordovician, Cambrian, and Archean: Wutai Group (Fig. 1).

The coal-bearing strata in this mine field are the Carboniferous Taiyuan Formation and Permian Shanxi Formation, with a total of 12 coal seams. The Shanxi Formation is 0–89.00 m thick, with an average of 54.30 m, and contains three coal seams, numbered Coal Nos. 1, 2, and 3. The Taiyuan Formation is 60.64–110.50 m thick, with an average thickness of 91.20 m, comprising eight coal seams: Coals Nos. 4–11 (Fig. 2). The most important minable coal beds in the southern part of the Antaibao open-pit mine were divided into No. 4^{-1} and No. 4^{-2}, however, in the northern part, they were combined into one bed of No. 4. Furthermore, the sedimentary environment of the coal-bearing strata was composed primarily of marine-continental transitional facies from the Carboniferous to Permian (Zhuang et al., 1998). The lower the coal seam, the greater the influence of seawater; therefore, the lower coal and coal gangue in the Taiyuan Formation contain more pyrite nodules

https://doi.org/10.1007/s42860-022-00211-7 Published online by Cambridge University Press

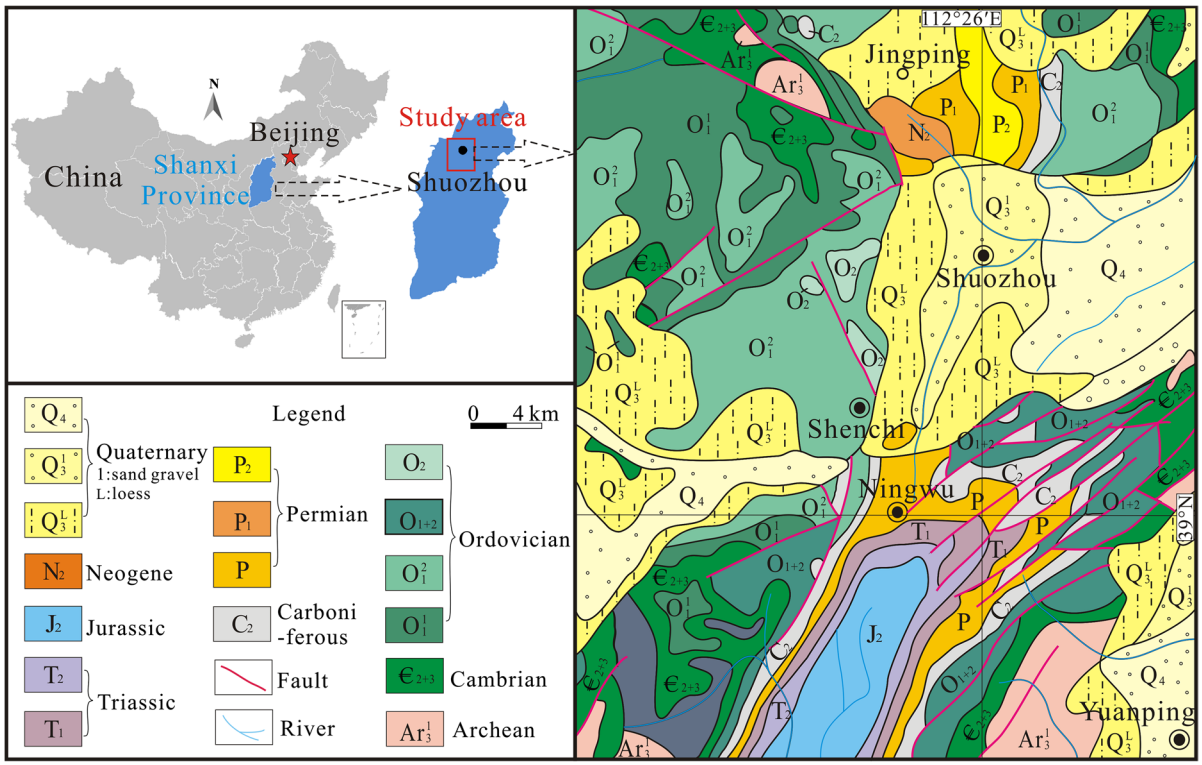

Fig. 1 Location and regional geological map of the study

(Qin et al., 2005). The main coal seams mined in the Pingshuo mining area were Nos. 4, 9, and 11.

Materials and Methods

Twenty-three coal gangue samples were collected from the Carboniferous Taiyuan Formation of the Pingshuo open-pit mine (Table 1). For coal gangue seams <20 cm thick, the full bed was collected. For thick coal gangue seams, the channel method was used for sampling. The samples for each ply were cut over an area 10 cm wide and 10 cm deep. Rock fragments collected per 20–30 cm height were bagged as one sample. The samples collected were sealed immediately in plastic bags in order to avoid contamination and to minimize oxidation.

The mineral composition of the bulk rock was determined via X-ray diffraction (XRD) on randomly oriented powder samples. The XRD measurements were carried out using a Rigaku (Tokyo, Japan) D/max-2500PC diffractometer equipped with CuKα radiation operated at 40 kV and 100 mA. The powders of bulk rocks were scanned using a continuous sweep method from 2.5 to 70°2θ at a scanning speed of 4°2θ min^{-1}. The quantitative analysis of mineral composition in the bulk rocks followed the method of Brindley (1980). The relative abundances of clay minerals were determined using their basal reflections and the mineral intensity factors of Moore and Reynolds (1989).

The morphology and occurrence state of minerals in the bulk rocks were observed using a CX40P polarizing microscope produced by Shunyu Optical Technology Co., Ltd (Zhejiang, China). The scanning electron microscope was equipped with an energy-dispersive X-ray spectrometer (SEM–EDS), which was used to investigate the morphology of the minerals, and also to determine the distribution of some elements. The powder and rock slice samples were stuck to an aluminum sample holder by sticky electronic-conductive carbon adhesive,

https://doi.org/10.1007/s42860-022-00211-7 Published online by Cambridge University Press

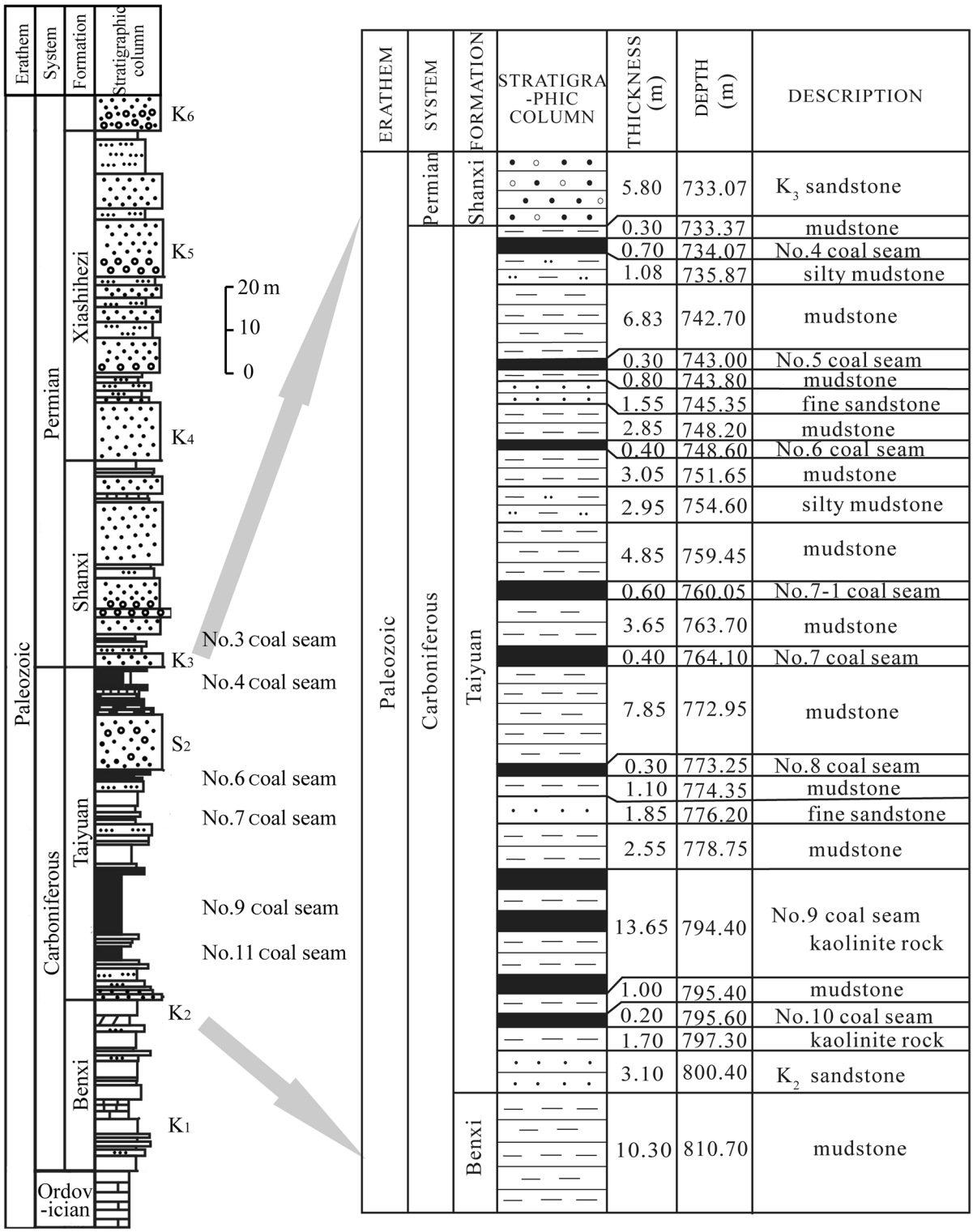

Fig. 2 Stratigraphic columns of the study area

https://doi.org/10.1007/s42860-022-00211-7 Published online by Cambridge University Press

Table 1 Source and characteristics of coal gangue samples

Coal field	Mining area	Sample No	Quantity	Source	Geological age
Pingshuo open-pit mine	Antaibao	ATB-4P	1	No. 4 coal	Carboniferous Taiyuan Formation
		ATB-4B	7	No. 4 coal seam floor	
		ATB-9P	3	No. 9 coal	
		ATB-9B	4	No. 9 coal seam floor	
	Anjialing	AJL-4P	6	No. 4 coal	
	Coal-preparation plant	TYF-PY	2	No. 8 coal (pyrite nodules)	

coated with a thin film of gold, and examined using an Hitachi (Tokyo, Japan) SU8020 and ZEISS GeminiSEM 300 field emission SEM.

Iron, which includes colloidal iron and ferruginous minerals, was removed from coal gangues by oxidation–reduction (Fig. 3). Most samples contain both Fe^{3+} and Fe^{2+}. Firstly, Fe^{2+} (e.g. FeS_2) was oxidized to Fe^{3+}, and then Fe^{3+} was reduced to soluble divalent iron salt by reduction. This method involved leaching the iron from the clay with oxalic acid, and reductive leaching by potent reducers, such as sodium dithionite (Ambikadevi & Lalithambika, 2000; Hosseini & Ahmadi, 2015). The changes in Fe content were determined before and after acid leaching. The major elements were measured using a PANalytical (Almelo, Netherlands) Axios-mAX wavelength dispersive X-ray fluorescence spectrometer (XRF) according to the national (Chinese) standard methods GB/T 14506.28–2010, GB/T 14506.34–2019, and GB/T 14506.14–2010.

Mössbauer analyses were conducted for samples at room temperature (RT) after acid leaching using a Mössbauer spectrometer (Wissel MVT-1000, Germany) with the radiation source of ^{57}Fe. The Mössbauer source was ^{57}Co with 25 mCi activity and the standard matrix was rhodium. The waveform mode was triangular wave, and the speed accuracy was ± 1.5%. The spectrum-solving program was *MossWinn 4.0*.

A Nicolet 6700 Continuum FTIR Microscope (micro-FTIR) (Thermo Scientific, Waltham, Massachusetts, USA) was used to scan over the range 650–4000 cm^{-1} to examine the specific bands of selected minerals in rock slices.

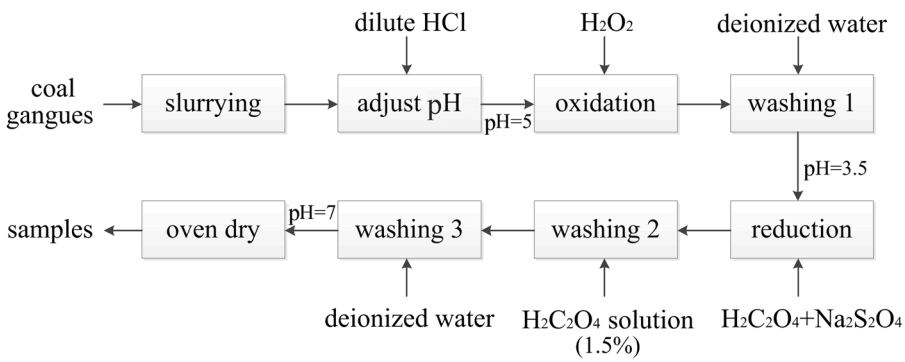

Fig. 3 A flow diagram of iron removal by the oxidation–reduction method

https://doi.org/10.1007/s42860-022-00211-7 Published online by Cambridge University Press

Results

Petrological and Mineralogical Analyses of Coal Gangue

The 23 coal-gangue samples collected were primarily mudstone, silty mudstone, and pelitic siltstone (Fig. 2). The XRD patterns of bulk-rock samples (Fig. 4) in Antaibao showed that the samples from Coals No. 4 and No. 9 consisted almost entirely of kaolinite, suggesting high purity. The rocks from the floors under Coals No. 4 and No. 9 were silty mudstone or pelitic siltstone, which were composed of kaolinite, quartz, feldspar, pyrite, illite, and magnesite. The weight percentage of detrital quartz varied from 10 to 50% (Table 2). The coal gangues with large pyrite contents, TYF-PY-1 and TYF-PY-2, selected by the coal preparation plant, were composed primarily of pyrite and marcasite, accompanied by small amounts of quartz and kaolinite. Compared with the standard JCPDS cards, the XRD pattern for the pyrite in coal gangue showed peaks at 28.54, 33.11, 37.16, 40.82, 47.44, and 56.35°2θ. Marcasite diffraction peaks, d_{110} = 0.344 nm and d_{101} = 0.269 nm, appeared at 25.91 and 33.25°2θ (Fig. 4).

The optical characteristics of the minerals in the coal gangue were observed using a polarizing microscope. Most mudstones were cryptocrystalline with no evident mineral particles (Fig. 5a). Some sandy mudstones had evident lamellar microstructures indicated weak water-current activity during the sedimentary process (Fig. 5b). Most of the clastic quartz had a small particle size, was well sorted, and had medium roundness. The interference color of kaolinite under cross-polarized light was gray; some grains were crystalline, and some had various clastic particles as a matrix. Vermiform kaolinite in coal gangue was observed under a polarizing microscope (Fig. 5c), and a some kaolinite crystal edges were weathered to boehmite (Fig. 5d). A small amount of

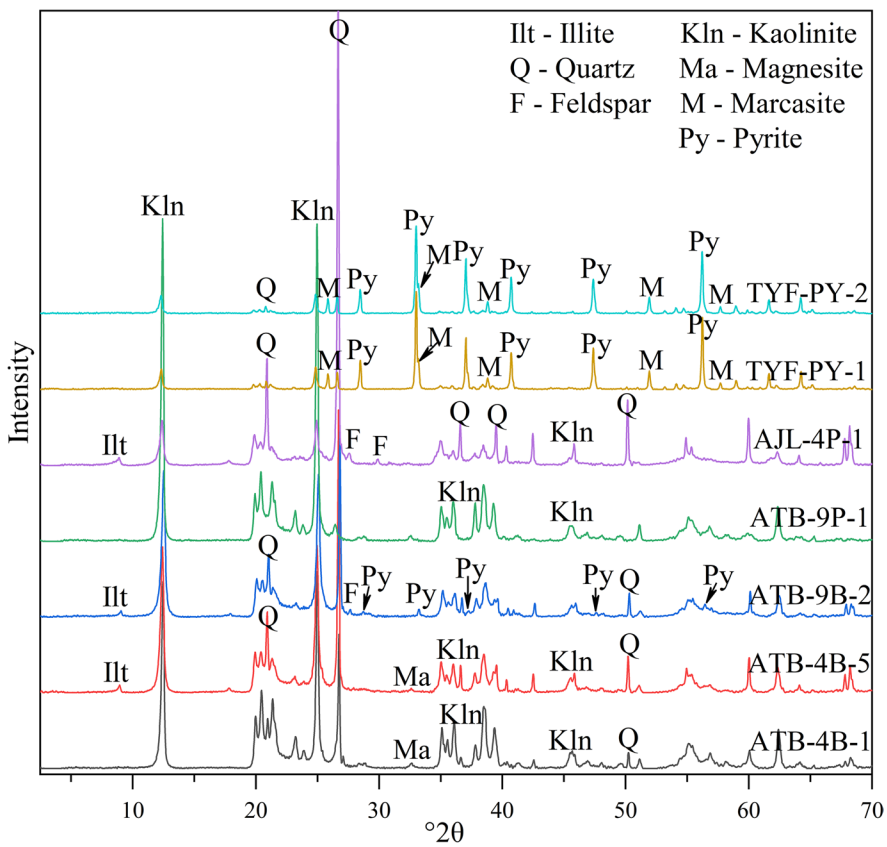

Fig. 4 XRD patterns of the bulk rocks of some samples

https://doi.org/10.1007/s42860-022-00211-7 Published online by Cambridge University Press

Table 2 Mineral composition and % fraction in samples from the study area

Sample No	Mineral content (wt.%)						
	Quartz	Feldspar	Pyrite	Magnesite	Marcasite	Illite	Kaolinite
ATB-4P-1							100.0
ATB-4B-1	15.9			2.9			81.2
ATB-4B-2	17.6			2.3			80.1
ATB-4B-3	26.4			1.0		0.8	72.6
ATB-4B-4	39.7			1.7		4.4	54.2
ATB-4B-5	33.6			1.8		4.6	60.0
ATB-4B-6	26.9						73.1
ATB-4B-7	10.5						89.5
ATB-9P-1							100.0
ATB-9P-2							100.0
ATB-9P-3							100.0
ATB-9B-1	14.1	0.4	30.9			6.2	48.4
ATB-9B-2	23.8	0.8	3.4			4.4	67.6
ATB-9B-3	12.1					3.3	84.6
ATB-9B-4	28.4	0.7	3.3			3.7	63.9
AJL-4P-1	48.9	2.1				3.0	46.0
AJL-4P-2	43.3	2.9		1.3		3.1	49.4
AJL-4P-3	42.5	1.6		1.1		2.1	52.7
AJL-4P-4	26.5	1.2		1.7		3.1	67.5
AJL-4P-5	12.2	0.3		2.0			85.5
AJL-4P-6	9.0			3.2			87.8
TYF-PY-1	3.7		66.5		9.6		20.2
TYF-PY-2	6.5		70.4		11.3		11.8

anorthoclase and mica was also observed (Fig. 5e). In the study area, the pyrite content in the lower coal seams of the Late Carboniferous Taiyuan Formation was large, e.g. in Coals Nos. 8 and 9, which was attributed to the influence of seawater on peat accumulation at the early stage of the Taiyuan Formation. The pyrite in the coal gangue was granular and black under plane-polarized light (Fig. 5f).

To identify the crystal morphology of pyrite and its relationship with other minerals in bulk rocks, coal gangue samples were observed via SEM (Fig. 6). Four different pyrite structures and morphologies were identified: (1) framboidal (Fig. 6a), (2) euhedral octahedral crystalline (Fig. 6b), (3) subhedral granular (Fig. 6c, d), and (4) irregular granular (Fig. 6c). Under the microscope, the framboidal pyrite was usually spherical or ellipsoidal, with a diameter of ~10 μm, and particles with a relatively complete crystal shape were arranged tightly in the sphere. The grain size of the octahedral crystals in the framboidal pyrite was 2–3 μm (Fig. 6a). In some coal gangues, pyrite exhibited a euhedral octahedral crystal form, and each single pyrite crystal was ~3–5 μm (Fig. 6b). Some subhedral granular pyrites had a particle size of 0.5–1.5 μm and were mixed with kaolinite (Fig. 6c, d).The pyrite nodules were massive, however, without a regular crystal structure. The surface of pyrite was not uniform and smooth, and the section was rectangular, square, or irregular (Fig. 6e). Kaolinite occurred primarily as lamellar crystals, with dimensions of 0.5–3 μm, and these crystals were in a single sheet or in sheets joined together with a vermiform texture (Fig. 6f).

https://doi.org/10.1007/s42860-022-00211-7 Published online by Cambridge University Press

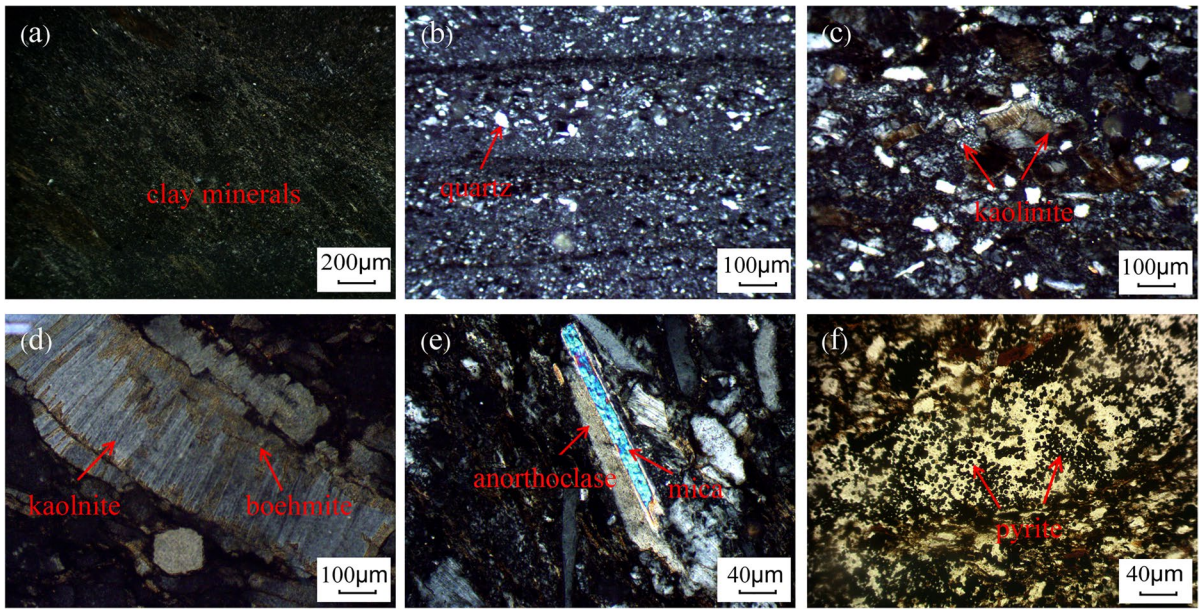

Fig. 5 Images of coal-gangue samples under **a-e** cross-polarized light and **f** plane polarized light: **a** cryptocrystalline mudstone in AJL-4P-5; **b** lamellar microstructure and terrigenous clastic quartz in sandy mudstone of ATB-9B-2; **c** vermiform kaolinite in ATB-4B-3; **d** the edge of kaolinite is weathered to boehmite in ATB-9P-2; **e** anorthoclase and mica in AJL-4P-4; **f** granular pyrite under plane polarized light in ATB-9B-1

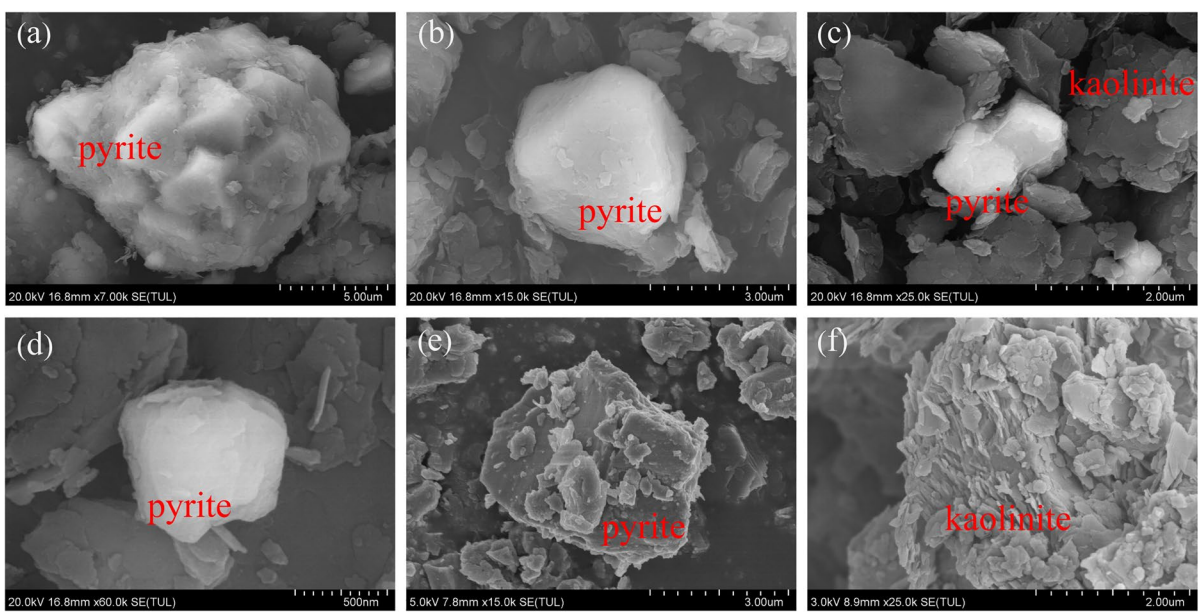

Fig. 6 SEM images of pyrite in coal gangue: **a** framboidal pyrite; **b** euhedral octahedral crystalline pyrite; **c**, **d** subhedral granular pyrite; **e** irregular granular pyrite; **f** kaolinite

https://doi.org/10.1007/s42860-022-00211-7 Published online by Cambridge University Press

Geochemical Characteristics

The concentrations of the major elements in the bulk-rock samples in the study area are given in Table 3. The SiO_2 and Al_2O_3 contents range from 35.31 to 64.86 wt.% and 17.83 to 34.70 wt.%, respectively. The mass ratio of SiO_2/Al_2O_3 (1.36–3.90) for the coal gangue samples was greater than the theoretical mass ratio of kaolinite (1.18) due to the high quartz content. In addition, small amounts of CaO, MgO, K_2O, and Na_2O could be related to illite and feldspar. The concentration of the main elements was consistent with the XRD results. The SO_2 content was greater in ATB-9B-1 (Table 3), indicating the presence of pyrite. The Fe_2O_3 contents in different samples varied greatly, ranging from 0.09 to 9.52 wt.%, with an average of 1.25 wt.%. In coal gangue samples without pyrite, the Fe_2O_3 content in Anjialing was greater than that in Antaibao. The loss on ignition (LOI) was 8.01 to 27.05 wt.%.

Analysis of Iron in the Minerals

Because coal gangue is such a heterogeneous material, with properties differing markedly according to the seam, exact studies of coal gangue are very important. Moreover, the atomic weight of the iron component in coal gangue was small. Mössbauer spectra, in conjunction with SEM, are convenient analytical tools for identification of the iron distribution in coal gangue with iron contents as small as 1 wt.%.

Coal gangue powder samples without pyrite, such as AJL-4P-3 (Fig. 7a), were analyzed with SEM–EDS. Surface scanning results showed that some clay minerals contained Fe (Fig. 7a-1). However, based on the brightness in the images, the Fe content was small, consistent with the geochemical test data in Table 2. In this batch of samples, the clay minerals consisted almost entirely of kaolinite. Consequently, kaolinite can be considered to be enriched in iron. Vermiform kaolinite and biotite-pseudomorphic kaolinite found in the rock slices were examined

Table 3 Chemical compositions of coal gangue samples from various mining areas (wt.%)

Sample No	SiO_2	Al_2O_3	*$Fe_2O_{3\ tot}$	TiO_2	CaO	MgO	K_2O	Na_2O	P_2O_5	SO_2	LOI	SiO_2/Al_2O_3
ATB-4P-1	48.01	34.58	0.23	0.49	0.07	0.03	0.07	0.03	0.02	0.06	16.35	1.39
ATB-4B-1	52.21	32.51	0.22	0.53	0.07	0.06	0.25	0.00	0.03	0.03	13.82	1.61
ATB-4B-2	51.28	33.62	0.18	0.55	0.07	0.03	0.12	0.00	0.04	0.01	13.99	1.53
ATB-4B-3	53.13	31.64	0.62	0.62	0.17	0.17	0.37	0.02	0.02	0.06	13.22	1.68
ATB-4B-4	54.76	28.40	0.66	1.11	0.10	0.20	0.81	0.00	0.05	0.14	13.45	1.93
ATB-4B-5	53.54	29.74	0.62	0.82	0.17	0.30	0.89	0.02	0.04	0.25	13.80	1.80
ATB-4B-6	56.49	26.04	0.66	1.20	0.10	0.22	0.88	0.02	0.05	0.12	14.89	2.17
ATB-4B-7	51.65	30.72	1.22	0.54	0.10	0.05	0.21	0.02	0.05	0.00	15.32	1.68
ATB-9P-1	47.58	34.70	0.13	0.47	0.05	0.05	0.18	0.02	0.02	0.13	16.48	1.37
ATB-9P-2	45.47	33.38	0.10	1.27	0.05	0.00	0.03	0.01	0.02	0.42	19.17	1.36
ATB-9P-3	46.56	34.12	0.09	0.71	0.05	0.02	0.05	0.01	0.01	0.22	18.12	1.36
ATB-9B-1	35.31	19.31	9.52	0.72	0.10	0.24	0.85	0.02	0.07	6.57	27.05	1.83
ATB-9B-2	51.62	29.03	1.16	1.23	0.11	0.18	0.74	0.01	0.05	0.64	15.04	1.78
ATB-9B-3	51.77	29.57	0.55	1.20	0.14	0.19	0.54	0.01	0.04	0.44	15.43	1.75
ATB-9B-4	50.75	24.44	2.21	1.14	0.10	0.16	0.85	0.02	0.04	1.53	18.61	2.08
AJL-4P-1	69.51	17.83	1.44	0.63	0.20	0.53	2.62	0.10	0.03	0.02	6.97	3.90
AJL-4P-2	64.82	21.07	1.35	0.63	0.24	0.59	2.58	0.12	0.04	0.02	8.40	3.08
AJL-4P-3	64.86	19.01	2.96	0.62	0.39	1.08	2.63	0.13	0.18	0.04	8.01	3.41
AJL-4P-4	50.06	26.61	1.01	1.16	0.17	0.25	1.16	0.05	0.10	0.13	19.04	1.88
AJL-4P-5	50.86	32.91	0.81	0.94	0.16	0.13	0.36	0.04	0.07	0.04	13.46	1.55
AJL-4P-6	49.70	34.01	0.50	0.98	0.13	0.07	0.15	0.02	0.04	0.02	14.21	1.46
Average	52.38	28.73	1.25	0.84	0.13	0.22	0.78	0.03	0.05	0.52	14.99	1.93

*$Fe_2O_{3\ tot}$—total iron

https://doi.org/10.1007/s42860-022-00211-7 Published online by Cambridge University Press

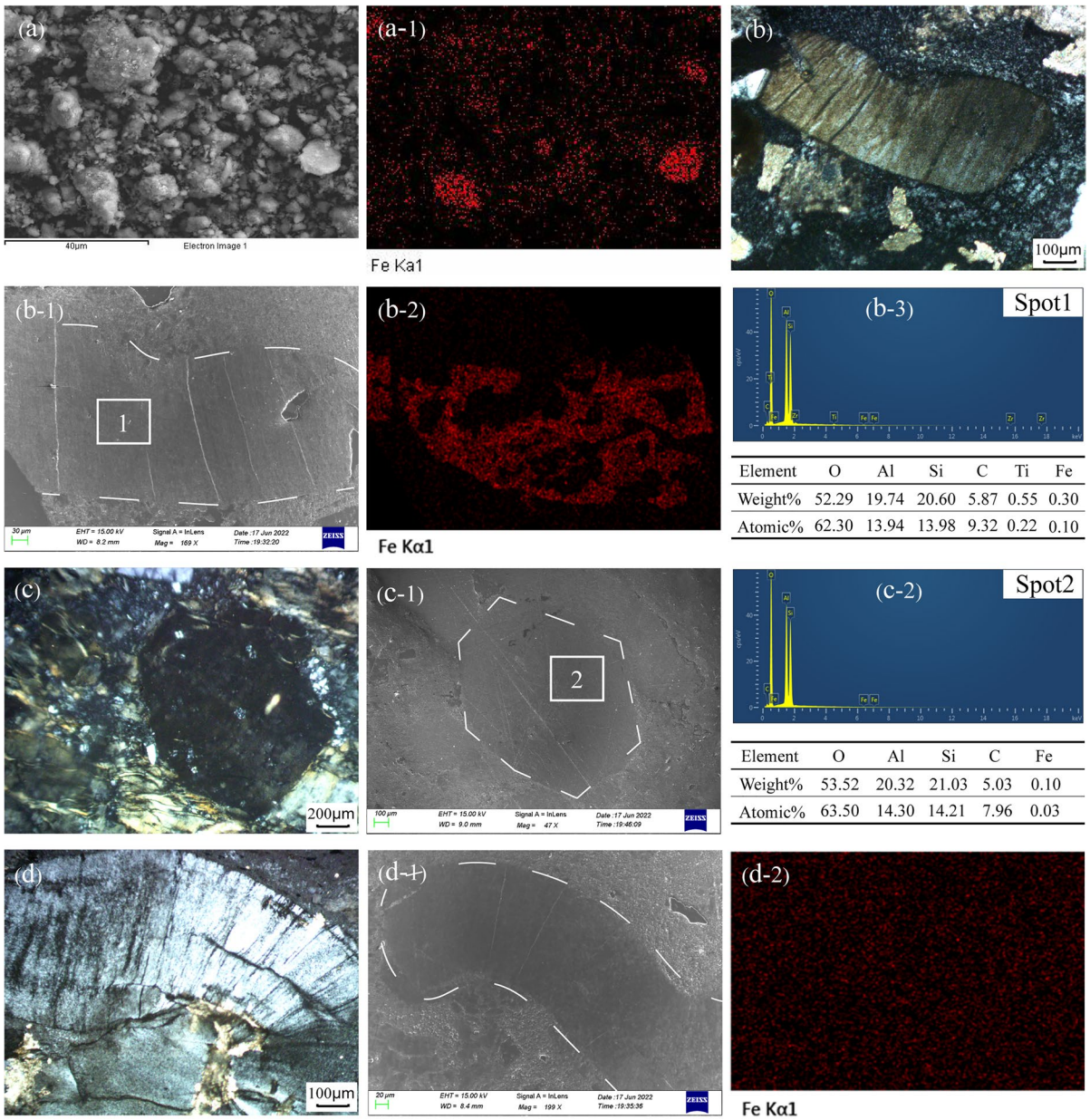

Fig. 7 Physical characteristics of kaolinite and spatial distribution of Fe: **a** SEM image of kaolinite in AJL-4P-3; (a-1) surface scanning of Fe from image **a**; **b** vermiform kaolinite under polarizing microscope; (b-1) SEM image of vermiform kaolinite; (b-2) surface scanning of Fe from image b-1; (b-3) EDS from spot 1; **c** biotite-pseudomorphic kaolinite under a polarizing microscope; (c-1) SEM image of biotite-pseudomorphic kaolinite; (c-2) EDS from spot 2; **d** vermiform kaolinite under polarizing microscope; (d-1) SEM image of a vermiform kaolinite; (d-2) surface scanning of Fe from image d-1

using a scanning electron microscope. A small number of vermiform kaolinites appeared brown (Fig. 7b) under a polarizing microscope, and the SEM–EDS results showed that kaolinite contained Fe. A surface scanning result (Fig. 7b-2) confirmed that iron was present mainly in the vermiform kaolinite (Fig. 7b-1), which was composed mainly of Si, Al, O, Ti, and Fe, with an Fe content of 0.3 wt.% (Fig. 7b-3). Furthermore, the SEM–EDS results showed that biotite-pseudomorphic kaolinite (Fig. 7c, c-1) also contained

https://doi.org/10.1007/s42860-022-00211-7 Published online by Cambridge University Press

a small amount of Fe (0.1 wt.%). The constituent elements of biotite-pseudomorphic kaolinite were Si, Al, O, and Fe (Fig. 7c-2). This iron-bearing kaolinite was probably derived from mica alteration. Most of the vermiform kaolinites were probably transformed from volcanic feldspar and did not contain iron, however. The vermiform kaolinites appeared clean and bright under a polarizing microscope (Fig. 7d); the surface scanning results, as shown in Figs. 7d-1 and d-2, showed no obvious iron aggregation, and these samples were composed mainly of Si, Al, and O.

Analysis of Mössbauer Spectra

The test results for the major elements showed that coal gangue contains both divalent iron (FeO) and trivalent iron (Fe_2O_3). Ferruginous minerals and colloidal iron in coal gangue were reduced to Fe^{2+} by oxidation–reduction, dissolved in solution, and then removed by acid leaching. The changes in the major elements before and after Fe removal are listed in Table 4. After removing the iron using this method, the iron content of samples ATB-4B-3, ATB-4B-5, AJL-4P-2, and AJL-4P-3 decreased slightly. That is, acid leaching removed a small amount of non-structural iron. Iron that cannot be washed off is part of the mineral that undergoes lattice substitution. In addition, the Fe^{2+} content in all samples was greater than that of Fe^{3+}.

The Mössbauer spectra of the samples after acid leaching are shown in Fig. 8. Differences in the spectra of the samples before and after iron removal are not significant. This may be due to the absence of ferruginous minerals in the samples, and the results of elemental tests showed very small amounts of iron removal. The Mössbauer spectra of the AJL-4P-3 sample consisted of Fe^{2+} and Fe^{3+}. The RT spectra showed an intense Fe^{3+} doublet with a narrow quadrupole splitting of ~0.628 mm s^{-1} and an isomer shift of 0.078 mm s^{-1} (relative to α-Fe) (Table 5). The bimodal result with an isomer shift of 0.818 mm s^{-1} and a quadrupole splitting moment of 2.605 mm s^{-1} was assigned to Fe^{2+}. The percentages of Fe^{3+} and Fe^{2+} were 26.93 and 73.07%, respectively. Similarly, the ATB-4B-3 sample consisted of Fe^{3+} and Fe^{2+} components in relative amounts of 52.22 and 47.78%, respectively. Studies have shown that the RT spectra have an intense Fe^{3+} doublet peak with a small quadrupole splitting of ~0.6 mm s^{-1} and an isomer shift of 0.24 mm s^{-1}, characteristic of iron contained in the structure of the clay minerals (Häusler, 2004; Waanders et al., 2003). Consequently, Fe ions are present in kaolinite, part of the coal gangue.

FTIR Spectroscopy

The micro-FTIR spectra of iron-containing and iron-free vermiform kaolinite in coal gangue (Fig. 9) revealed four notable, well defined, characteristic bands at 3694, 3669, 3652, and 3620 cm^{-1}, assigned to structural OH stretching vibrations. Among them, the two stretching vibration peaks at 3694 and 3620 cm^{-1} had greater intensities and were sharp, both of which were attributed to the outer and inner hydroxyl groups of kaolinite, respectively. The 1000–1200 cm^{-1} absorption bands (999 and 1031 cm^{-1}, 1004 and 1022 cm^{-1}) in the mid-frequency zone belong to the stretching vibration of Si–O. A sharp absorption peak near 912 cm^{-1} and a weak absorption peak near 935 cm^{-1} were observed,

Table 4 Chemical compositions of coal gangue samples before and after iron removal (wt.%)

Treatment conditions	Sample No	SiO_2	Al_2O_3	*$Fe_2O_{3\ tot}$	TiO_2	CaO	MgO	K_2O	Na_2O	P_2O_5	FeO	LOI
Raw ore	ATB-4B-3	53.13	31.64	0.62	0.62	0.17	0.17	0.37	0.02	0.02	0.50	13.22
	ATB-4B-5	53.54	29.74	0.62	0.82	0.17	0.30	0.89	0.02	0.04	0.52	13.80
	AJL-4P-2	64.82	21.07	1.35	0.63	0.24	0.60	2.58	0.12	0.04	0.88	8.40
	AJL-4P-3	64.86	19.01	2.96	0.62	0.39	1.08	2.63	0.13	0.18	2.04	8.01
After iron removal	ATB-4B-3	53.53	31.48	0.59	0.69	0.11	0.17	0.35	< 0.01	0.02	0.48	12.93
	ATB-4B-5	53.57	29.59	0.58	0.81	0.12	0.26	0.87	0.03	0.04	0.47	13.97
	AJL-4P-2	67.78	19.78	1.15	0.69	0.15	0.54	2.65	0.12	0.03	0.67	7.05
	AJL-4P-3	67.24	18.38	2.69	0.68	0.23	1.05	2.73	0.09	0.09	1.87	6.77

*$Fe_2O_{3\ tot}$—total iron

https://doi.org/10.1007/s42860-022-00211-7 Published online by Cambridge University Press

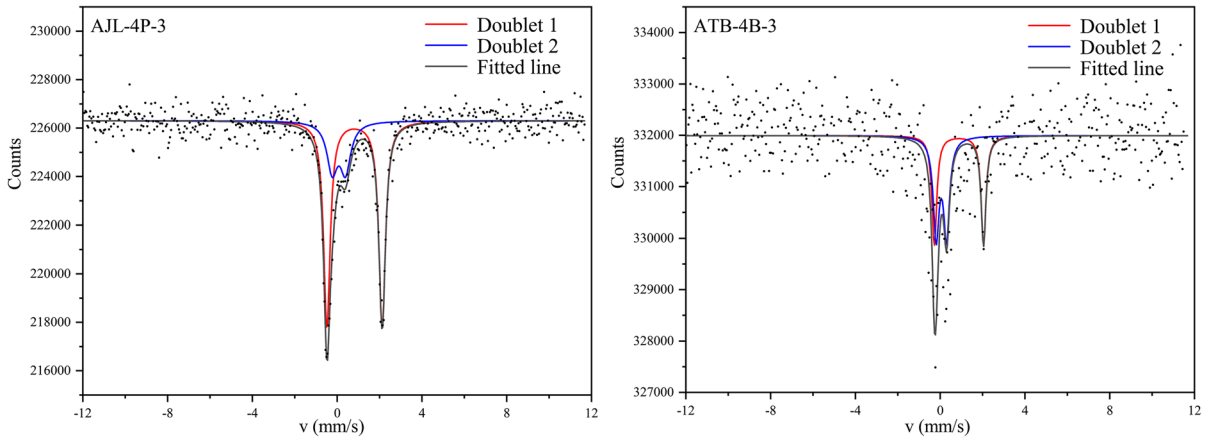

Fig. 8 Mössbauer spectra of samples after iron removal

and were attributed to the bending vibrations of the internal and external hydroxyl groups, respectively.

Interestingly, the micro-FTIR spectra of the iron-containing vermiform kaolinite had a few weak absorption peaks in the range of 3500–3600 cm^{-1} (Fig. 9a), whereas the ordinary vermiform kaolinite did not (Fig. 9b). Among them, represented by two peaks at 3555 and 3565 cm^{-1}, may be the vibrations of the chemical bonds associated with Fe.

Discussion

Coal gangue is a mixture of various rocks and minerals which have small carbon contents. It is used widely in building materials, developing soil, energy, underground backfills, and other industries (Li & Wang, 2019). The recycling of coal gangue is considered an eco-friendly alternative that not only addresses its disposal, but also contributes to the cost-efficient and sustainable use of resources. However, owing to the different lithological and mineralogical compositions of the coal-bearing strata deposited in various coal-accumulating periods, the composition of coal gangue varies, showing certain regional differences. The composition of coal gangue determines how it can be used.

The coal-bearing strata in the study area include the Permian Shanxi Formation, the Carboniferous Taiyuan Formation, and the Benxi Formation. Furthermore, the sedimentary depositional environment of the coal-bearing strata was mainly marine-continental transitional facies during the Carboniferous to Permian. Coal gangues Nos. 4 and 9 in Antaibao contain few impurities, and the kaolinite is high-purity. The No. 4 coal gangue in Anjialing, No. 4 coal seam floor, and No. 9 coal seam floor in Antaibao are silty mudstone or pelitic siltstone, composed mainly of kaolinite, quartz, feldspar, pyrite, illite, and magnesite. The formation of coal seams Nos. 9–11 was affected significantly by

Table 5 Mössbauer parameters for the main iron-bearing phases in coal gangue

Sample No	Species	IS ($mm\ s^{-1}$)	QS ($mm\ s^{-1}$)	LW ($mm\ s^{-1}$)	A (%)	χ^2
AJL-4P-3	Fe^{2+}	0.818	2.605	0.374	73.07	1.017
	Fe^{3+}	0.078	0.628	0.597	26.93	
ATB-4B-3	Fe^{2+}	0.882	2.320	0.277	47.78	1.297
	Fe^{3+}	0.056	0.491	0.336	52.22	

IS – Isomer shift; QS – Quadrupole splitting; LW – Line width; A – Relative area

https://doi.org/10.1007/s42860-022-00211-7 Published online by Cambridge University Press

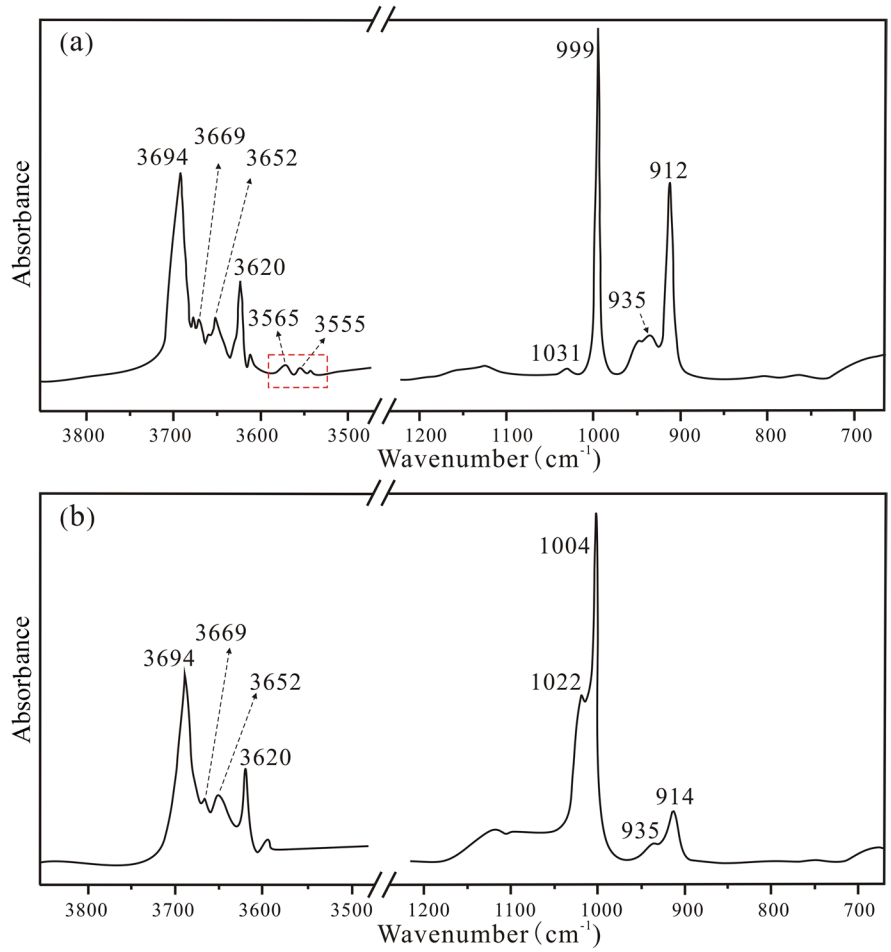

Fig. 9 FTIR spectra of **a** iron-containing and **b** iron-free kaolinite

seawater, resulting in a large amount of pyrite and sulfur in the No. 9 coal floor of Antaibao.

The occurrence states of Fe in coal gangue primarily include ferruginous minerals, colloidal state ($Fe(OH)_3$), and crystal-lattice substitution (Fe^{2+} or Fe^{3+}). Ferruginous minerals in coal gangue include mainly siderite, hematite, pyrite, marcasite, goethite, magnetite, and ilmenite (Bertolino et al., 2010), which can be identified easily using XRD and SEM. However, colloidal state and crystal-lattice substitution are not easy to distinguish from one another, and the substitution sites of the ions in the crystal lattice are also unknown. This restricts high-value utilization of those coal gangue materials.

Ferruginous Minerals

The XRD and SEM results showed that the ferruginous minerals found in the Pingshuo open-pit mine were pyrite and marcasite. A small amount of marcasite was found in the No. 8 coal gangue. Marcasite and pyrite are polymorphic sulfide minerals with the same chemical composition; pyrite is cubic and marcasite is orthorhombic. Some scholars (Shi et al., 2011) found a small amount of siderite in the coal gangue of the No. 4 coal seam floor.

Similar to most sedimentary pyrites (Frankie & Hower, 1987; Querol et al., 1989), the types of pyrite found in coal and coal gangue were: massive pyrite, homogeneous nodular and in clusters; framboidal

https://doi.org/10.1007/s42860-022-00211-7 Published online by Cambridge University Press

pyrite, appearing in inorganic and bacteriogenic forms; euhedral pyrite, which is either isolated or clustered; and disseminated pyrite, in its infilling and replacement varieties (Dai et al., 2003; Kortenski & Kostova, 1996; Tang & Ren, 1996). Structurally, the most developed types are disseminated, layered, nodular, and veins. Microscopically, most of pyrites are colloidal, biological structure-filling, and granular. In the sampled section of the Pingshuo open-pit mine, pyrite in the Carboniferous coal gangue was primarily layered and nodular, and a small amount of disseminated and vein pyrite was also found. Under a polarizing microscope and using SEM, the morphologies and structures of pyrite in the coal gangue were primarily framboidal, euhedral granular, subhedral granular, and irregular granular (Fig. 6).

Pyrite is a product of a strongly reducing environment, and various types of pyrite in coal gangue are products of different environments (Devic et al., 2010). Most of the euhedral, framboidal, and massive pyrite formed during peat deposition. Anhedral replacement pyrite formed in the peat bed during early diagenesis. Disseminated pyrite-filled fractures and cleats were formed during diagenesis, catagenesis, and metagenesis (Liu et al., 1998; Tang & Ren, 1996). In the Pingshuo open-pit mine, euhedral, subhedral, framboidal, and massive pyrite in the Carboniferous coal gangue indicate that they were formed during peat deposition. The euhedral crystals and framboidal pyrite were mainly octahedral, which was the most stable state of pyrite (Tang & Ren, 1993), indicating that pyrite crystals were formed in a stable medium environment with low supersaturation. The coal-forming environment was affected by seawater, and the supply of S^{-} and Fe^{2+} was sufficient and in a supersaturated state. Pyrite and marcasite coexisted, indicating that the medium was moderately acidic.

Colloidal State of Fe

Except for a small amount of coal gangue containing pyrite and marcasite, most coal gangues do not contain ferruginous minerals, but Fe still appears in the lists of major elements. It indicates that Fe may exist in rocks and minerals in the form of colloidal state or crystal-lattice substitution, and the results of major elements showed that coal gangue contains both Fe^{2+} and Fe^{3+}.

The SEM–EDS results showed that the coal gangue powder samples without ferruginous minerals contained Fe (Fig. 7a, a-1). However, owing to the small Fe content (0.1–2.96 wt.%), the image brightness of Fe was less. The results of the major element analysis after iron removal from coal gangue by the oxidation–reduction method showed that the iron content decreased (Table 4). Nevertheless, samples such as ATB-4B-3, ATB-4B-5, AJL-4P-2, and AJL-4P-3 had no ferruginous minerals. This indicated that the reduced iron content in the sample was colloidal. However, even if non-structurally bound iron was removed by acid leaching, the sample still contained a small amount of iron. This was the iron ion of the crystal-lattice substitution in kaolinite. The crystal-lattice substitution of iron in kaolinite is both divalent and trivalent, and the Fe^{2+} content is greater than that of Fe^{3+} (Fig. 10). The formation environment of coal gangue is conducive to the survival of divalent iron ions, which is probably the reason for the large Fe^{2+} content.

Crystal-Lattice Substitution of Fe

The SEM–EDS analysis showed that coal gangues contain two types of kaolinite: iron-containing and iron-free. Iron-free kaolinite (Fig. 7d, d-1, d-2), which looks clean and bright and may be transformed from volcanic feldspar, makes up the vast majority of samples. Some kaolinites contain small amounts of Fe (0.1 and 0.3 wt.%), e.g. vermiform kaolinite (Fig. 7b)

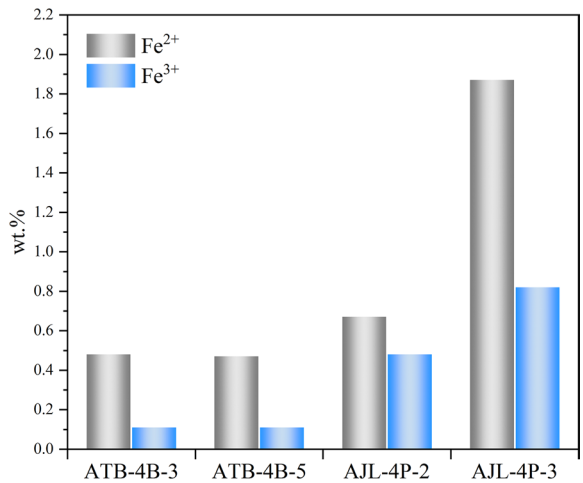

Fig. 10 Comparison of the amounts of Fe^{2+} and Fe^{3+} in crystal lattices of various samples

https://doi.org/10.1007/s42860-022-00211-7 Published online by Cambridge University Press

and biotite-pseudomorphic kaolinite (Fig. 7c), which appear brown under a polarizing microscope and are probably transformed from volcanic biotite. Because the rock slices are cut to the interior of the mineral (Fig. 7b, c, d), this part of the Fe exists within the kaolinite mineral in the form of lattice substitution. The micro-FTIR spectra (Fig. 9) confirmed that iron-containing vermiform kaolinite had a few weak absorption peaks in the 3500–3600 cm^{-1} range compared to iron-free vermiform kaolinite. This phenomenon also confirmed that Fe underwent lattice substitution in kaolinite.

Kaolinite is a typical 1:1 layered dioctahedral silicate mineral with the chemical formula $Al_2[Si_2O_5](OH)_4$. The silicon-oxygen tetrahedra and aluminum-oxygen octahedra are staggered by sharing oxygen atoms to form an asymmetric crystal layer unit (Liu et al., 2016; Zhou et al., 2019). Research (Chen et al., 2020; Fysh et al., 1983; Pierre et al., 1992; Yang & Ding, 2005) has shown that there are three types of structural iron occupation in kaolinite: (1) hexa-coordinated Fe^{2+} – Fe^{2+} replaces Al^{3+} in the aluminum-oxygen octahedra (Fig. 11a); (2) hexa-coordinated Fe^{3+} – Fe^{3+} replaces Al^{3+} in the aluminum-oxygen octahedra (Fig. 11b); and (3) tetra-coordinated Fe^{3+} – Fe^{3+} replaces Si^{4+} in the silica-oxygen tetrahedra (Fig. 11c).

In the current study, samples AJL-4P-3 and ATB-4B-3 contained mainly two types of occupied Fe: (1) the bimodal with isomer shifts of 0.818 and 0.882 mm s^{-1} and quadrupole splitting moments of 2.605 and 2.320 mm s^{-1} was assigned as hexa-coordinated Fe^{2+} (Fe^{2+} substituted for kaolinite aluminum-oxygen octahedral Al^{3+}) (Fig. 11a); (2) the bimodal with isomer shifts of 0.078 and 0.056 mm s^{-1} (relative to α-Fe) and quadrupole splitting moments of 0.628 and 0.491 mm s^{-1} was assigned as tetra-coordinated Fe^{3+} (Fe^{3+} substituted kaolinite silicon-oxygen tetrahedral Si^{4+}) (Fig. 11c); the percentages of hexa-coordinated Fe^{2+} were 73.07 and 47.78%, and those of tetra-coordinated Fe^{3+} were 26.93 and 52.22%, respectively (Table 5).

Kaolinite exhibits a dioctahedral structure. Trivalent cations (Al^{3+}) are within the octahedral sheets, occupying only 2/3 of the octahedral sites, the remainder being vacant. The ionic radius of Al^{3+} is 0.51 Å, and the ionic radii of Fe^{2+} and Fe^{3+} are 0.74 and 0.64 Å, respectively. Consequently, the substitution of iron in the kaolinite lattice is possible. The condition for cations to enter the interlayer domain is that higher-valence ions are replaced by lower-valence ions, resulting in an insufficient positive charge in the structural cells. In the Pingshuo open-pit mine, two types of iron appear in the mineral crystal lattice: tetra-coordinated Fe^{3+} and hexa-coordinated Fe^{2+}. Hexa-coordinated Fe^{3+} was not found in the study area. Therefore, the degree of replacement of Fe in kaolinite of the coal measures might vary from 'easy' to 'difficult': Fe^{2+} replaced Al^{3+} in the aluminum-oxygen octahedra > Fe^{3+} substituted Si^{4+} in the silica-oxygen tetrahedra > Fe^{3+} replaced Al^{3+} in the aluminum-oxygen octahedra. This is similar to the study by Chen et al. (2020) on iron occupation of kaolin in coal measures of Anhui, China, and the study by Pierre et al. (1992) on the iron of soil kaolins from southwestern Australia. In nature, however, the type and amount of iron occupation in kaolinite may be affected by many factors, including the formation conditions of kaolinite, the sedimentary environment, and the type and amount of Fe ions in the environment. This should be analyzed according to the specific situation.

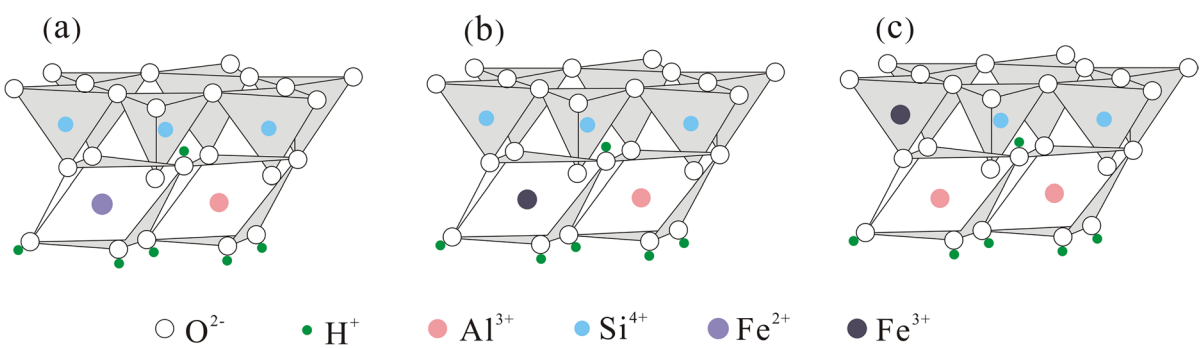

Fig. 11 Three types of substitution site for Fe in kaolinite (after Zhou et al., 2019)

https://doi.org/10.1007/s42860-022-00211-7 Published online by Cambridge University Press

Conclusions

In the Pingshuo open-pit mine, the coal gangues are mudstones, silty mudstones, and pelitic siltstones. Their mineralogical composition is primarily kaolinite and quartz, with a small amount of feldspar, pyrite, illite, and magnesite. Pyrite was enriched locally to form pyrite nodules. Iron occurs in three states in coal gangue: as ferruginous minerals, as crystal-lattice substitution, and a small amount in a colloidal state. In a strongly reducing environment, Fe can combine with S to form minerals such as pyrite and marcasite, and the morphologies of pyrite are primarily framboidal, euhedral octahedral, subhedral granular, and irregular. When the S content is small, Fe enters the crystal lattice of the mineral or forms a colloidal state. The lattice substitution of minerals in coal gangue occurs mainly in kaolinite, resulting in two types of kaolinite in coal gangue: iron-containing and iron-free. Iron occurs in two states in kaolinite: (1) hexa-coordinated Fe^{2+}; and (2) tetra-coordinated Fe^{3+}. The degree of replacement of Fe in coal measures kaolinite, from easy to difficult, is: Fe^{2+} replaces Al^{3+} in the aluminum-oxygen octahedra, Fe^{3+} replaces Si^{4+} in the silica-oxygen tetrahedra, and Fe^{3+} replaces Al^{3+} in the aluminum-oxygen octahedra.

Acknowledgements This authors are grateful for financial support by the National Key R&D Program of China (No. 2019YFC1904903) and the Science and Technology Major Projects of Shanxi Province of China (No. 20181101003).

Funding Funding sources are as stated in the Acknowledgments.

Declarations

Conflicts of Interest The authors declare that they have no conflict of interest.

References

Ambikadevi, V. R., & Lalithambika, M. (2000). Effect of organic acids on ferric iron removal from iron-stained kaolinite. *Applied Clay Science, 16*(3–4), 133–145.

Bertolino, L. C., Rossi, A. M., Scorzelli, R. B., & Torem, M. L. (2010). Influence of iron on kaolin whiteness: An electron paramagnetic resonance study. *Applied Clay Science, 49*, 170–175.

Brindley, G. W. (1980). Quantitative X-ray analysis of clays. In G. W. Brindley & G. Brown (Eds.), *Crystal structures of clay minerals and their X-ray identification* (pp. 411–438). Mineralogical Society.

Cao, Y., Ma, B., & Fu, G. (2021a). Research progress of high value utilization of coal gangue. *Refractories & Lime, 46*, 35–39.

Cao, Z., Jia, Y., Wang, Q., & Cheng, H. (2021b). High-efficiency photo-fenton Fe/g-C_3N_4/kaolinite catalyst for tetracycline hydrochloride degradation. *Applied Clay Science, 212*, 106213.

Chen, J., Min, F., Liu, L., & Cai, C. (2020). Systematic exploration of the interactions between Fe-doped kaolinite and coal based on DFT calculations. *Fuel, 266*, 117082.

Cheng, H., Liu, Q., Huang, M., Zhang, S., & Frost, R. L. (2013). Application of TG-FTIR to study SO_2 evolved during the thermal decomposition of coal-derived pyrite. *Thermochimica Acta, 555*, 1–6.

Dai, S., Ren, D., Tang, Y., Shao, L., & Li, S. (2002). Distribution, isotopic variation and origin of sulfur in coals in the Wuda coalfield, Inner Mongolia, China. *International Journal of Coal Geology, 51*, 237–250.

Dai, S., Hou, X., Ren, D., & Tang, Y. (2003). Surface analysis of pyrite in the no. 9 coal seam, Wuda coalfield, Inner Mongolia, China, using high-resolution time-of-flight secondary ion mass-spectrometry. *International Journal of Coal Geology, 55*, 139–150.

Devic, G., Pfendt, P., Jovancicevic, B., & Popovic, Z. (2010). Pyrite formation in organic-rich clay, calcitic and coal-forming environments. *Acta Geologica Sinica, 80*, 574–588.

Frankie, K., & Hower, J. (1987). Variation in pyrite size, form, and microlithotype association in the springfield (no. 9) and herrin (no. 11) coals, Western Kentucky. *International Journal of Coal Geology, 7*, 349–364.

Fysh, S. A., Cashion, J. D., & Clark, P. E. (1983). Mössbauer effect studies of iron in kaolin. II. Surface iron. *Clays and Clay Minerals, 31*, 293–298.

Gonzalez, J. A., & Ruiz, M. (2006). Bleaching of kaolins and clays by chlorination of iron and titanium. *Applied Clay Science, 33*, 219–229.

Häusler, W. (2004). Firing of clays studied by X-ray diffraction and Mössbauer spectroscopy. *Hyperfine Interactions, 154*, 121–141.

Hosseini, M. R., & Ahmadi, A. (2015). Biological beneficiation of kaolin: A review on iron removal. *Applied Clay Science, 107*, 238–245.

Kortenski, J., & Kostova, I. (1996). Occurrence and morphology of pyrite in Bulgarian coals. *International Journal of Coal Geology, 29*, 273–290.

Kramer, M. J., Mendelev, M. I., & Napolitano, R. E. (2010). In situ observation of antisite defect formation during crystal growth. *Physical Review Letters, 105*, 245501.

Li, J., & Wang, J. (2019). Comprehensive utilization and environmental risks of coal gangue: A review. *Journal of Cleaner Production*, *239*.

Liu, D., Yang, Q., Zhou, C., Tang, D., & Kang, X. (1998). Occurrence and geological genesis of pyrites in Late Paleozoic coals in North China. *Chinese Journal of Geochemistry, 28*, 340–350.

Liu, Q., Li, X., & Cheng, H. (2016). Insight into the self-adaptive deformation of kaolinite layers into nanoscrolls. *Applied Clay Science, 124–125*, 175–182.

Liu, Y., Yu, L., & Wang, H. (2013). Study on countermeasures of coal gangue pollution prevention and regional sustainable development in China. In *Applied Mechanics and Materials* (Vol. 307, pp. 510–513). Trans Tech Publications, Ltd.

Lu, Y., Li, J., & Liu, Q. (2015). Effect of grain size and crystallinity of kaolinite from coal on kaolinite intercalation. *Acta Mineralogica Sinica, 35*, 209–213.

Meng, F., Yu, J., Tahmasebi, A., & Han, Y. (2013). Pyrolysis and combustion behavior of coal gangue in O_2/CO_2 and O_2/N_2 mixtures using TGA and drop tube furnace. *Energy & Fuels, 27*, 2923–2932.

Moore, D. M., & Reynolds, R. C., Jr. (1989). *X-ray diffraction and the Identification and Analysis of Clay Minerals*. Oxford University Press.

Ozdeniz, A. H., Corumluoglu, O., & Kalayci, I. (2010). The relationship between the natural compaction and the spontaneous combustion of industrial-scale coal stockpiles. *Energy Sources, 22*, 121–129.

Pierre, T. G. S., Singh, B., Webb, J., & Gilkes, B. (1992). Mössbauer spectra of soil kaolins from South-Western Australia. *Clays and Clay Minerals, 40*, 341–346.

Pone, J. D. N., Hein, K. A. A., Stracher, G. B., Annegarn, H. J., Finkleman, R. B., Blake, D. R., Mccormack, J. K., & Schroeder, P. (2007). The spontaneous combustion of coal and its by-products in the Witbank and Sasolburg coalfields of South Africa. *International Journal of Coal Geology, 72*, 124–140.

Qin, Y., Wang, W., Song, D., & Zhang, X. (2005). Geochemistry characteristics and sedimentary micro-environments of no. 11 coal seam of the Taiyuan Formation of upper Carboniferous in Pingshuo mining district, Shanxi Province. *Journal of Palaeogeography, 7*, 249–260.

Querol, X., Chinchon, S., & Lopez-Soler, A. (1989). Iron sulfide precipitation sequence in Albian coals from the Maestrazgo basin, southeastern Iberian range, Northeastern Spain. *International Journal of Coal Geology, 11*, 171–189.

Querol, X., Zhuang, X., Font, O., Izquierdo, M., Alastuey, A., Castro, I., Drooge, B. L. V., Moreno, T., Grimalt, J. O., & Elvira, J. (2011). Influence of soil cover on reducing the environmental impact of spontaneous coal combustion in coal waste gobs: A review and new experimental data. *International Journal of Coal Geology, 85*, 2–22.

Ribeiro, J., Silva, E. F. D., Li, Z., Ward, C., & Flores, D. (2010). Petrographic, mineralogical and geochemical characterization of the serrinha coal waste pile (Douro coalfield, Portugal) and the potential environmental impacts on soil, sediments and surface waters. *International Journal of Coal Geology, 83*, 456–466.

Shao, Q. (2007). The impact of heavy metals transfer from coal waste rock to soil in Xinzhuangzi subsidence area. *Coal Geology & Exploration, 6*, 34–37.

Shi, L., Liu, Q., Zhang, Z., & Yu, X. (2011). Characteristics and genesis of coal measures kaolinite in late Paleozoic of Pingshuo mining area. In *Proceedings of the Proceedings of the 13th annual meeting of the Chinese society of mineral and rock geochemistry* (pp. 322).

Soliman, M. F., & Goresy, A. E. (2012). Framboidal and idiomorphic pyrite in the upper Maastrichtian sedimentary rocks at Gabal Oweina, Nile Valley, Egypt: Formation processes, oxidation products and genetic implications to the origin of framboidal pyrite. *Geochimica et Cosmochimica Acta, 90*, 195–220.

Spears, D. A., Tarazona, M., & Lee, S. (1994). Pyrite in UK coals: Its environmental significance. *Fuel, 73*, 1051–1055.

Stracher, G. B., & Taylor, T. P. (2004). Coal fires burning out of control around the world: Thermodynamic recipe for environmental catastrophe. *International Journal of Coal Geology, 59*, 7–17.

Tang, Y., & Ren, D. (1993). Research on different pyrites in late Permian coal of Sichuan Province, southwestern China. *Coal Science and Technology, 21*, 37–45.

Tang, Y., & Ren, D. (1996). The genesis of pyrites in coal. *Geological Review, 42*, 64–70.

Waanders, F. B., Vinken, E., Mans, A., & Mulaba-Bafubiandi, A. F. (2003). Iron minerals in coal, weathered coal and coal ash–SEM and mössbauer results. *Hyperfine Interactions, 148–149*, 21–29.

Yang, X., & Ding, S. (2005). Study on kaolin in coal measures of west Beijing by mössbauer spectroscopy. *Journal of Hebei Institute of Architectural Science and Technology, 22*, 73–75.

Yani, S., & Zhang, D. (2010). An experimental study into pyrite transformation during pyrolysis of Australian lignite samples. *Fuel, 89*, 1700–1708.

Zhou, C., Liu, G., Yan, Z., Fang, T., & Wang, R. (2012). Transformation behavior of mineral composition and trace elements during coal gangue combustion. *Fuel, 97*, 644–650.

Zhou, Y., LaChance, A. M., Smith, A. T., Cheng, H., Liu, Q., & Sun, L. (2019). Strategic design of clay-based multifunctional materials: From natural minerals to nanostructured membranes. *Advanced Functional Materials, 29*, 1807611.

Zhuang, X., Zeng, R., & Xu, W. (1998). Trace elements in no. 9 coal from Antaibao open pit mine, Pingshuo, Shanxi province. *Earth Science-Journal of China University of Geosciences, 23*, 40–45.